Wind and Structures, *Vol. 24, No. 3 (2017) 267-285*
DOI: https://doi.org/10.12989/was.2017.24.3.267

Frequency and critical fluid velocity analysis of pipes reinforced with FG-CNTs conveying internal flows

M.M. Ghaitani and A. Majidian*

Department of Mechanical Engineering, Sari Branch, Islamic Azad University, Sari, Iran

(Received November 18, 2016, Revised December 30, 2016, Accepted January 3, 2017)

Abstract. This paper addresses vibration and instability of embedded functionally graded (FG)-carbon nanotubes (CNTs)-reinforced pipes conveying viscous fluid. The surrounding elastic medium is modeled by temperature-dependent orthotropic Pasternak medium. Flugge shell model is applied for mathematical modeling of structure. Based on energy method and Hamilton's principal, the motion equations are derived. Differential quadrature method (GDQM) is applied for obtaining the frequency and critical fluid velocity of system. The effects of different parameters such as volume percent of CNTs, elastic medium, boundary condition and geometrical parameters are discussed.

Keywords: nonlinear vibration; Flugge shell model; orthotropic Pasternak medium; FG-CNT-reinforced pipe; DQM

1. Introduction

Recently, CNTs are used as a reinforcing constituent instead of conventional fibers in composite structures due to their special material properties. Therefore, the introduction of CNTs into a polymer matrix may greatly improve mechanical properties of the resulting nanocomposites, such as tensile strength and elastic modulus. However, these structures have wide application in many micro-electro-mechanical systems (MEMS) and the mechanical analyses of them are essential.

The mechanical analysis of nano-composite structures has attracted considerable attention in recent years. 3D free vibration analysis of homogenous isotropic circular cylindrical shells was investigated by Khalili *et al*. (2012) using refined higher-order shear deformation theory (RHOST). Nascimbene (2013) studied optimization and advanced numerical computation of a sail fiber-reinforced composite model to increase the performance of a yacht under wind action. Leiw *et al*. (2014) used meshless approach for postbuckling analysis of CNT-reinforced-FG (CNTR-FG) cylindrical panels based on the arc-length method combined with the modified Newton–Raphson method. Based on kp-Ritz method and the Eshelby-Mori-Tanaka approach, Zhang *et al*. (2014a) presented large deflection geometrically nonlinear behaviour of CNTR-FG cylindrical panels. Lei *et al*. (2014) studied dynamic stability analysis of CNTR-FG cylindrical panels based on the Eshelby–Mori–Tanaka approach and the first-order shear deformation theory. Zhang *et al*. (2014b)

*Corresponding author, Dr., E-mail: a_majidian@yahoo.com

http://www.techno-press.org/?journal=was&subpage=8 ISSN: 1226-6116 (Print), 1598-6225 (Online)

investigated free vibration of CNTR-FG cylindrical panels based on the first-order shear deformation shell theory. Stresses due to bending behavior of functionally graded carbon nanotube-reinforced (FGCNTR) open cylindrical shells subjected to mechanical loads was studied by Jafari Mehrabadi and Sobhani Aragh (2014). Nonlocal nonlinear buckling analysis of embedded polymeric temperature-dependent microplates resting on an elastic matrix as orthotropic temperature-dependent elastomeric medium was investigated by Kolahchi *et al*. (2015). Thomas and Roy (2016) presented vibration analysis of functionally graded CNTR-FG shell structures using an eight-noded shell element considering transverse shear effect according to Mindlin's hypothesis. Kolahchi *et al*. (2016) investigated nonlinear dynamic stability analysis of embedded temperature-dependent viscoelastic plates reinforced by single-walled carbon nanotubes (SWCNTs).

None of the above researchers have considered instability of structures induced by internal fluid. In the field of cylindrical shell conveying fluid, Amabili *et al*. (2002, 2009) presented stability of circular cylindrical shells containing inviscid, incompressible fluid with and without considering geometric imperfections. Both a Finite Volume and a Discrete Vortex technique to solve the unsteady Navier-Stokes equations were employed by Morgenthal and McRobie (2002) to study the air flow around long-span bridge decks. A formulation, based on the semi-analytical finite element method, was proposed by Senthil Kumar and Ganesan (2008) for elastic conical shells conveying fluids. A fluid–structure interaction model for stability analysis of shells conveying fluid was developed by Firouz-Abadi *et al.* (2010) using the linearized Bernoulli equation for unsteady pressure on the fluid–shell interface. The unsteady fluid-structure interaction (FSI) problems with large structural displacement were solved by HE (2015) using partitioned solution approaches in the arbitrary Lagrangian-Eulerian finite element framework. Nonlinear theoretical model for cantilevered micropipes/microbeams conveying fluid was developed by Hu *et al.* (2016) to explore the possible size-dependent nonlinear responses based on the modified couple stress theory. Monte Carlo simulation method was used by Alizadeh *et al*. (2016) in conjunction with finite elements for probabilistic self-excited vibration and stability analyses of pipes conveying fluid. The flow-induced vibration characteristics (natural frequency and critical flow velocity) of FGM cylindrical shells partially resting on elastic foundation were investigated by Park and Kim (2016) using an analytical method.

In the present study, nonlinear vibration and instability of FG-CNT-reinforced pipes resting on orthotropic Pasternak medium are investigated. The pipe is conveying viscous fluid. The nonlinear governing equations are obtained based on Hamilton's principal along with Flugge shell theory. DQM is applied for obtaining the frequency and critical fluid velocity of the pipe. The effects of the volume percent of CNTs, Pasternak medium, CNTs distribution type and boundary conditions on the frequency and critical fluid velocity of the pipe are disused in detail.

2. Formulation

2.1 Mixture rule

As shown in Fig. 1, a FG-CNT-reinforced (FG-CNTR) cylindrical shell with length L and thickness h is considered. The CNTRC cylindrical shell is surrounded by an orthotropic Pasternak medium which is simulated by K_W, $K_{g\xi}$ and $K_{g\eta}$ correspond Winkler foundation parameter, shear foundation parameters in ξ and η directions, respectively.

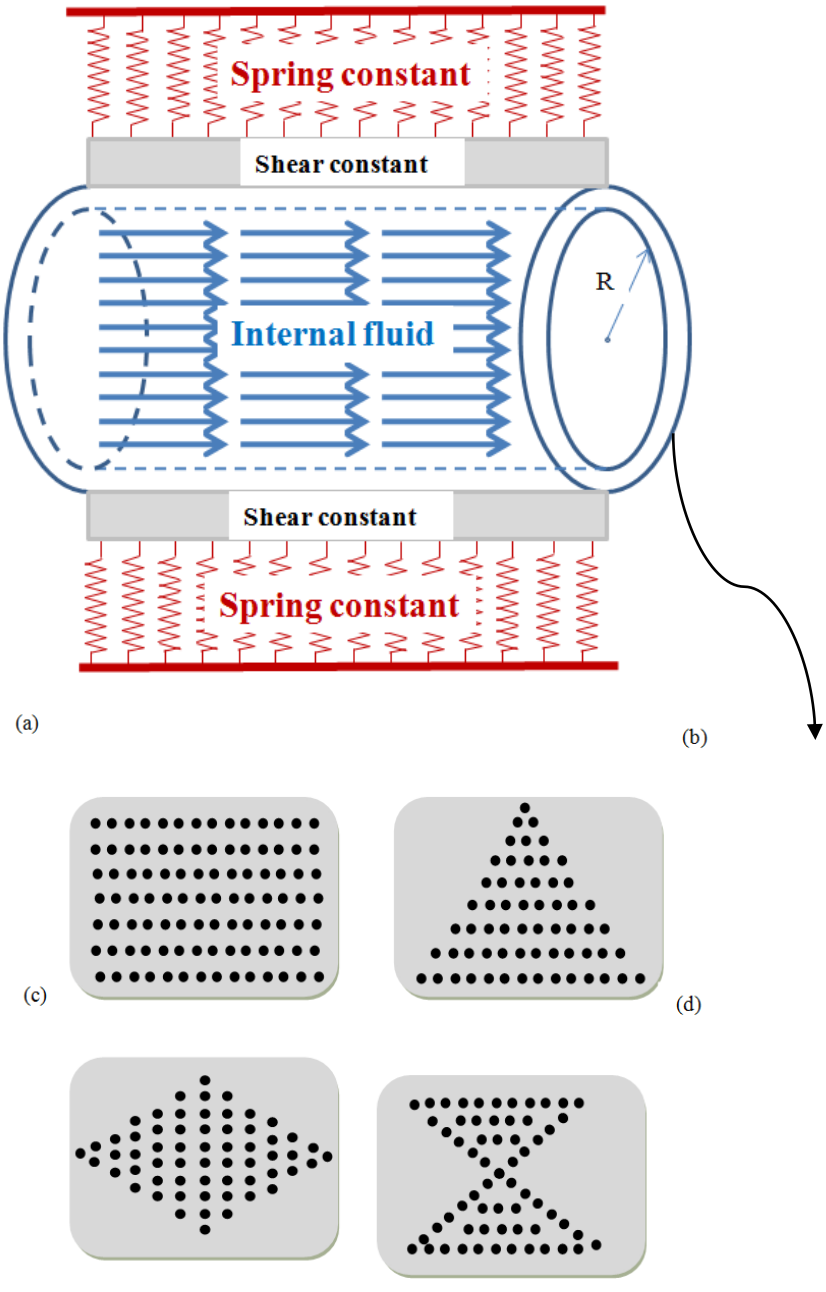

Fig. 1 A schematic figure of FG-CNT-reinforced pipe embedded in elastic medium (a) UD, (b) FGA, (c) FGO and (d) FGX

Four types of CNTRC cylindrical shell namely as uniform distribution (UD) along with three types of FG distributions (FGA, FGO, FGX) of CNTs along the thickness direction of a CNTRC cylindrical shell are considered. In order to obtain the equivalent material properties two-phase nanocomposites (i.e., polymer as matrix and CNT as reinforcer), the rule of mixture is applied. According to mixture rule, the effective Young and shear moduli of CNTRC cylindrical shell can be written as (Zhang *et al*. 2014a)

$$E_{11} = \eta_1 V_{CNT} E_{r11} + (1 - V_{CNT}) E_m, \tag{1a}$$

$$\frac{\eta_2}{E_{22}} = \frac{V_{CNT}}{E_{r22}} + \frac{(1 - V_{CNT})}{E_m}, \tag{1b}$$

$$\frac{\eta_3}{G_{12}} = \frac{V_{CNT}}{G_{r12}} + \frac{(1 - V_{CNT})}{G_m}, \tag{1c}$$

where E_{r11}, E_{r22} and G_{r11} indicate the Young's moduli and shear modulus of SWCNTs, respectively, and E_m, G_m represent the corresponding properties of the isotropic matrix. With the knowledge that load transfer between the nanotube and polymeric phases is less than perfect (e.g. the surface effects, strain gradients effects, intermolecular coupled stress effects, etc.), we introduced η_j (j= 1, 2, 3) into Eqs. (1(a))- (1(c)) to consider the size-dependent material properties. η_j is called the CNT efficiency parameter which will be determined later by matching the elastic modulus of CNTRCs observed from the MD simulation results with the numerical results obtained from the rule of mixture. The scale-dependent material properties, η_j (j= 1, 2, 3), can be calculated by matching the effective properties of CNTRC obtained from the MD simulations with those from the rule of mixture. V_{CNT} and V_m are the volume fractions of the CNTs and matrix, respectively, which the sum of them equals to unity. The uniform and three types of FG distributions of the CNTs along the thickness direction of the CNTRC cylindrical shells take the following forms

$$UD: \quad V_{CNT} = V_{CNT}^*, \tag{2a}$$

$$FGV: \quad V_{CNT}(z) = \left(1 - \frac{2z}{h}\right) V_{CNT}^*, \tag{2b}$$

$$FGO: \quad V_{CNT}(z) = 2\left(1 - \frac{2|z|}{h}\right) V_{CNT}^*, \tag{2c}$$

$$FGX: \quad V_{CNT}(z) = 2\left(\frac{2|z|}{h}\right) V_{CNT}^*, \tag{2d}$$

where

$$V_{CNT}^* = \frac{w_{CNT}}{w_{CNT} + (\rho_{CNT} / \rho_m) - (\rho_{CNT} / \rho_m) w_{CNT}}, \tag{3}$$

where w_{CNT}, ρ_m and ρ_{CNT} are the mass fraction of the CNT, the densities of the matrix and CNT, respectively. Similarly, the thermal expansion coefficients in the longitudinal and transverse directions respectively (α_{11} and α_{22}), Poisson's ratio (ν_{12}) and the density (ρ) of the CNTRC cylindrical shell can be determined as

$$\nu_{12} = V_{CNT}^{*}\nu_{r12} + V_{m,}\nu_{m}, \tag{4}$$

$$\rho = V_{CNT}^{*}\rho_{r} + V_{m,}\rho_{m,}, \tag{5}$$

$$\alpha_{11} = V_{CNT}^{*}\alpha_{r11} + V_{m,}\alpha_{m,}, \tag{6}$$

$$\alpha_{22} = (1+\nu_{r12})V_{CNT}\alpha_{r22} + (1+\nu_{m})V_{m}\alpha_{m} - \nu_{12}\alpha_{11}, \tag{7}$$

where ν_{r12} and ν_m are Poisson's ratios of the CNT and matrix, respectively. In addition, α_{r11}, α_{r22} and α_m are the thermal expansion coefficients of the CNT and matrix, respectively. It should be noted that ν_{12} is assumed as constant over the thickness of the FG-CNTRC cylindrical shells.

2.2 Basic equations

Based on Flugge shell theory, the displacement field can be expressed as (Amabili 2008)

$$\begin{aligned} u_x(x,\theta,z,t) &= u\ (x,\theta,t) - z\frac{\partial}{\partial x}w\ (x,\theta,t), \\ u_\theta(x,\theta,z,t) &= v(x,\theta,t) - z\frac{\partial}{R\partial\theta}w\ (x,\theta,t), \\ u_z(x,\theta,z,t) &= w(x,\theta,t), \end{aligned} \tag{8}$$

where (u_x, u_θ, u_z) denote the displacement components at an arbitrary point (x, θ, z) in the pipe, and (u, v, w) are the displacement of a material point at (x, θ) on the mid-plane (i.e., $z = 0$) of the pipe along the *x*-, θ-, and *z*-directions, respectively..

The von Kármán strains associated with the above displacement field can be expressed in the following form

$$\begin{Bmatrix} \varepsilon_{xx} \\ \varepsilon_{\theta\theta} \\ \gamma_{x\theta} \end{Bmatrix} = \begin{Bmatrix} \varepsilon_{xx}^{0} \\ \varepsilon_{\theta\theta}^{0} \\ \gamma_{x\theta}^{0} \end{Bmatrix} + z\begin{Bmatrix} \varepsilon_{xx}^{1} \\ \varepsilon_{\theta\theta}^{1} \\ \gamma_{x\theta}^{1} \end{Bmatrix}, \tag{9}$$

where

$$\begin{Bmatrix} \varepsilon_{xx}^0 \\ \varepsilon_{\theta\theta}^0 \\ \varepsilon_{x\theta}^0 \end{Bmatrix} = \begin{Bmatrix} \dfrac{\partial u}{\partial x} + \dfrac{1}{2}\left(\dfrac{\partial w}{\partial x}\right)^2 \\ \dfrac{\partial v}{R\partial\theta} + \dfrac{w}{R} + \dfrac{1}{2}\left(\dfrac{\partial w}{R\partial\theta}\right)^2 \\ \dfrac{\partial v}{\partial x} + \dfrac{\partial u}{R\partial\theta} + \dfrac{\partial w}{\partial x}\dfrac{\partial w}{R\partial\theta} \end{Bmatrix}, \tag{10}$$

$$\begin{Bmatrix} \varepsilon_{xx}^1 \\ \varepsilon_{\theta\theta}^1 \\ \varepsilon_{x\theta}^1 \\ \varepsilon_{xz}^1 \\ \varepsilon_{\theta z}^1 \end{Bmatrix} = \begin{Bmatrix} \dfrac{\partial^2 w}{\partial x^2} \\ \dfrac{\partial^2 w}{R^2\partial\theta^2} - \dfrac{\partial v}{R^2\partial\theta} \\ \dfrac{2\partial^2 w}{R\partial\theta\partial x} - \dfrac{2\partial v}{R\partial x} \end{Bmatrix}, \tag{11}$$

where $(\varepsilon_{xx}, \varepsilon_{\theta\theta})$ are the normal strain components and $(\gamma_{x\theta})$ are the shear strain components.

The constitutive equation for stresses $\boldsymbol{\sigma}$ and strains $\boldsymbol{\varepsilon}$ matrix in thermal environment may be written as follows

$$\begin{Bmatrix} \sigma_{xx} \\ \sigma_{\theta\theta} \\ \sigma_{x\theta} \end{Bmatrix} = \begin{Bmatrix} C_{11} & C_{12} & 0 \\ C_{12} & C_{22} & 0 \\ 0 & 0 & C_{66} \end{Bmatrix} \begin{Bmatrix} \varepsilon_{xx} \\ \varepsilon_{\theta\theta} \\ \gamma_{x\theta} \end{Bmatrix}, \tag{12}$$

2.3 Energy method

The total potential energy,V , of the FG pipe is the sum of strain energy, U , kinetic energy, K , and the work done by the elasomeric medium, W .

The strain energy can be written as

$$U = \frac{1}{2}\int_{\Omega_0}\int_{-h/2}^{h/2}\left(\sigma_{xx}\varepsilon_{xx} + \sigma_{\theta\theta}\varepsilon_{\theta\theta} + \sigma_{x\theta}\gamma_{x\theta}\right)dV \tag{13}$$

Combining of Eqs. (5)-(10) and (12) yields

$$\begin{aligned} U = \frac{1}{2}\int_{\Omega_0}\Bigg(& N_{xx}\left(\frac{\partial u}{\partial x} + \frac{1}{2}\left(\frac{\partial w}{\partial x}\right)^2\right) + N_{\theta\theta}\left(\frac{\partial v}{\partial\theta} + \frac{w}{R} + \frac{1}{2}\left(\frac{\partial w}{R\partial\theta}\right)^2\right) + Q_\theta\left(\frac{\partial w}{R\partial\theta} + \psi_\theta\right) \\ & + N_{x\theta}\left(\frac{\partial v}{\partial x} + \frac{\partial u}{R\partial\theta} + \frac{\partial w}{\partial x}\frac{\partial w}{R\partial\theta}\right) - M_{xx}\left(\frac{\partial^2 w}{\partial x^2}\right) - M_{\theta\theta}\left(\frac{\partial^2 w}{R^2\partial\theta^2} - \frac{\partial v}{R^2\partial\theta}\right) - M_{x\theta}\left(\frac{2\partial^2 w}{R\partial\theta\partial x} - \frac{2\partial v}{R\partial x}\right)\Bigg)dx d\theta, \end{aligned} \tag{14}$$

where the stress resultant-displacement relations can be written as

$$\begin{Bmatrix} N_{xx} \\ N_{\theta\theta} \\ N_{x\theta} \end{Bmatrix} = \int_{-h/2}^{h/2} \begin{bmatrix} \sigma_{xx} \\ \sigma_{\theta\theta} \\ \sigma_{x\theta} \end{bmatrix} dz, \tag{15}$$

$$\begin{Bmatrix} M_{xx} \\ M_{\theta\theta} \\ M_{x\theta} \end{Bmatrix} = \int_{-h/2}^{h/2} \begin{bmatrix} \sigma_{xx} \\ \sigma_{\theta\theta} \\ \sigma_{x\theta} \end{bmatrix} z dz, \tag{16}$$

Substituting Eqs. (9)-(12) into Eqs. (15) and (16), the stress resultant-displacement relations can be obtained as follow

$$\begin{aligned}
N_{xx} &= A_{11}\left(\frac{\partial u}{\partial x}+\frac{1}{2}\left(\frac{\partial w}{\partial x}\right)^2\right)+A_{12}\left(\frac{\partial v}{R\partial\theta}+\frac{w}{R}+\frac{1}{2}\left(\frac{\partial w}{R\partial\theta}\right)^2\right)-B_{11}\left(\frac{\partial^2 w}{\partial x^2}\right)-B_{12}\left(\frac{\partial^2 w}{R^2\partial\theta^2}-\frac{\partial v}{R^2\partial\theta}\right),\\
N_{\theta\theta} &= A_{12}\left(\frac{\partial u}{\partial x}+\frac{1}{2}\left(\frac{\partial w}{\partial x}\right)^2\right)+A_{22}\left(\frac{\partial v}{R\partial\theta}+\frac{w}{R}+\frac{1}{2}\left(\frac{\partial w}{R\partial\theta}\right)^2\right)-B_{12}\left(\frac{\partial^2 w}{\partial x^2}\right)-B_{22}\left(\frac{\partial^2 w}{R^2\partial\theta^2}-\frac{\partial v}{R^2\partial\theta}\right),\\
N_{x\theta} &= A_{66}\left(\frac{\partial u}{R\partial\theta}+\frac{\partial v}{\partial x}+\frac{\partial w}{\partial x}\frac{\partial w}{R\partial\theta}\right)-B_{66}\left(\frac{2\partial^2 w}{R\partial\theta\partial x}-\frac{2\partial v}{R\partial x}\right),
\end{aligned} \tag{17}$$

$$\begin{aligned}
M_{xx} &= B_{11}\left(\frac{\partial u}{\partial x}+\frac{1}{2}\left(\frac{\partial w}{\partial x}\right)^2\right)+B_{12}\left(\frac{\partial v}{R\partial\theta}+\frac{w}{R}+\frac{1}{2}\left(\frac{\partial w}{R\partial\theta}\right)^2\right)-D_{11}\left(\frac{\partial^2 w}{\partial x^2}\right)-D_{12}\left(\frac{\partial^2 w}{R^2\partial\theta^2}-\frac{\partial v}{R^2\partial\theta}\right),\\
M_{\theta\theta} &= B_{12}\left(\frac{\partial u}{\partial x}+\frac{1}{2}\left(\frac{\partial w}{\partial x}\right)^2\right)+B_{22}\left(\frac{\partial v}{R\partial\theta}+\frac{w}{R}+\frac{1}{2}\left(\frac{\partial w}{R\partial\theta}\right)^2\right)-D_{12}\left(\frac{\partial^2 w}{\partial x^2}\right)-D_{22}\left(\frac{\partial^2 w}{R^2\partial\theta^2}-\frac{\partial v}{R^2\partial\theta}\right),\\
M_{x\theta} &= B_{66}\left(\frac{\partial u}{R\partial\theta}+\frac{\partial v}{\partial x}+\frac{\partial w}{\partial x}\frac{\partial w}{R\partial\theta}\right)-D_{66}\left(\frac{2\partial^2 w}{R\partial\theta\partial x}-\frac{2\partial v}{R\partial x}\right),
\end{aligned} \tag{18}$$

where

$$A_{ij} = \int_{-h/2}^{h/2} C_{ij} dz, \qquad (i, j = 1,2,6) \tag{19}$$

$$B_{ij} = \int_{-h/2}^{h/2} C_{ij} z dz, \tag{20}$$

$$D_{ij} = \int_{-h/2}^{h/2} C_{ij} z^2 dz, \tag{21}$$

The kinetic energy of system may be written as

$$K = \frac{\rho}{2}\int_{\Omega_0}\int_{-h/2}^{h/2}\left(\left(\dot{u}_x\right)^2+\left(\dot{u}_\theta\right)^2+\left(\dot{u}_z\right)^2\right)dV \tag{22}$$

The external work due to Pasternak medium and fluid can be written as

$$W = \int_0^L \left(P_{Fluid} + P_{Elastic}\right) w dx, \tag{23}$$

2.4 Fluid flow work

Consider the flow of fluid in a FG pipe in which the flow is assumed to be axially symmetric, Newtonian, laminar and fully developed. The basic momentum governing equation of the flow simplifies to (Wang and Ni 2009)

$$\rho_b \frac{\partial v_r}{\partial t} = -\frac{\partial P}{\partial r} + \frac{1}{r}\frac{\partial \tau_{r\theta}}{\partial \theta} - \frac{\tau_{\theta\theta}}{r} + \frac{\partial \tau_{xr}}{\partial x}, \tag{24}$$

where ρ_b and P are fluid mass density and flow fluid pressure, respectively. The fluid force acted on the FG pipe can be calculated from Eq. (24). Since the velocity and acceleration of the pipe and fluid at the point of contact between them are equal (Wang and Ni 2009), we have

$$v_r = \frac{dw}{dt}, \tag{25}$$

where

$$\frac{d}{dt} = \frac{\partial}{\partial t} + v_x \frac{\partial}{\partial x}, \tag{26}$$

where v_x is the mean flow velocity. In Eq. (24), shear stress (τ) is dependent to viscosity μ which can be expressed as follows

$$\tau_{r\theta} = \mu \frac{1}{r}\frac{\partial v_r}{\partial \theta}, \tag{27}$$

$$\tau_{\theta\theta} = 2\mu \frac{v_r}{r}, \tag{28}$$

$$\tau_{rx} = \mu \frac{\partial v_r}{\partial x}, \tag{29}$$

Finally, using Eqs. (25)-(29) and combination with Eq. (24), the fluid flow work may be written as

$$q_{Fluid} = \left[-\rho_f h_f \left(\frac{\partial^2 w}{\partial t^2} + 2v_x \frac{\partial^2 w}{\partial x \partial t} + v_x^2 \frac{\partial^2 w}{\partial x^2} \right) + \frac{h_f}{R^2}\frac{\partial}{\partial \theta}\left(\mu \left(\frac{\partial^2 w}{\partial \theta \partial t} + v_x \frac{\partial^2 w}{\partial \theta \partial x} \right) \right) \right.$$
$$\left. -\frac{2h_f}{R}\left(\mu \left(\frac{\partial w}{\partial t} + v_x \frac{\partial w}{\partial x} \right) \right) + h_f \frac{\partial}{\partial x}\left(\mu \left(\frac{\partial^2 w}{\partial x \partial t} + v_x \frac{\partial^2 w}{\partial x^2} \right) \right) \right], \tag{30}$$

where ρ_f is density of fluid.

2.5 Orthotropic Pasternak foundation

The external force of orthotropic Pasternak medium can be expressed as (Kutlu and Omurtag 2012)

$$P = K_W w - K_{g\xi}\left(\cos^2\theta\frac{\partial^2 w}{\partial x^2} + 2\cos\theta\sin\theta\frac{\partial^2 w}{R\partial x\partial\theta} + \sin^2\theta\frac{\partial^2 w}{R^2\partial\theta^2}\right) - K_{g\eta}\left(\sin^2\theta\frac{\partial^2 w}{\partial x^2} - 2\sin\theta\cos\theta\frac{\partial^2 w}{R\partial x\partial\theta} + \cos^2\theta\frac{\partial^2 w}{R^2\partial\theta^2}\right), \tag{31}$$

where K_W, $K_{g\xi}$ and $K_{g\eta}$ are spring constant of Winkler type, shear constant in ξ and η directions, respectively; angle θ describes the local ξ direction of orthotropic foundation with respect to the global x-axis of the pipe.

2.6 Governing equations

The governing equations can be derived by Hamilton's principal as follows

$$\int_0^t (\delta U - \delta W - \delta K)dt = 0. \tag{32}$$

Substituting Eqs. (17), (22) and (23) into Eq. (32) yields the following governing equations

$$\delta u: \frac{\partial N_{xx}}{\partial x} + \frac{\partial N_{x\theta}}{R\partial\theta} = \rho h\frac{\partial^2 u}{\partial t^2}, \tag{33}$$

$$\delta v: \frac{\partial N_{x\theta}}{\partial x} + \frac{\partial N_{\theta\theta}}{R\partial\theta} + \frac{\partial M_{\theta\theta}}{R^2\partial\theta} + \frac{\partial M_{x\theta}}{R\partial x} = \rho h\frac{\partial^2 v}{\partial t^2}, \tag{34}$$

$$\delta w: \frac{\partial^2 M_{xx}}{\partial x^2} + \frac{\partial^2 M_{\theta\theta}}{R^2\partial\theta^2} + \frac{2\partial^2 M_{x\theta}}{R\partial x\partial\theta} - \frac{N_{\theta\theta}}{R} + \left[-\rho_f h_f\left(\frac{\partial^2 w}{\partial t^2} + 2v_x\frac{\partial^2 w}{\partial x\partial t} + v_x^2\frac{\partial^2 w}{\partial x^2}\right) + \frac{h_f}{R^2}\frac{\partial}{\partial\theta}\left(\mu\left(\frac{\partial^2 w}{\partial\theta\partial t} + v_x\frac{\partial^2 w}{\partial\theta\partial x}\right)\right) - \frac{2h_f}{R}\left(\mu\left(\frac{\partial w}{\partial t} + v_x\frac{\partial w}{\partial x}\right)\right) + h_f\frac{\partial}{\partial x}\left(\mu\left(\frac{\partial^2 w}{\partial x\partial t} + v_x\frac{\partial^2 w}{\partial x^2}\right)\right)\right] - K_W w + K_{g\xi}\left(\cos^2\theta\frac{\partial^2 w}{\partial x^2} + 2\cos\theta\sin\theta\frac{\partial^2 w}{R\partial x\partial\theta} + \sin^2\theta\frac{\partial^2 w}{R^2\partial\theta^2}\right) + K_{g\eta}\left(\sin^2\theta\frac{\partial^2 w}{\partial x^2} - 2\sin\theta\cos\theta\frac{\partial^2 w}{R\partial x\partial\theta} + \cos^2\theta\frac{\partial^2 w}{R^2\partial\theta^2}\right) = \rho h\frac{\partial^2 w}{\partial t^2}, \tag{35}$$

Substituting Eqs. (17) and (18) into Eqs. (33) to (35), the governing equations can be written as follow

$$\delta u: \frac{\partial}{\partial x}\left(A_{11}\left(\frac{\partial u}{\partial x}+\frac{1}{2}\left(\frac{\partial w}{\partial x}\right)^2\right)+A_{12}\left(\frac{\partial v}{R\partial\theta}+\frac{w}{R}+\frac{1}{2}\left(\frac{\partial w}{R\partial\theta}\right)^2\right)-B_{11}\left(\frac{\partial^2 w}{\partial x^2}\right)-B_{12}\left(\frac{\partial^2 w}{R^2\partial\theta^2}-\frac{\partial v}{R^2\partial\theta}\right)\right)$$
$$+\frac{\partial}{R\partial\theta}\left(A_{66}\left(\frac{\partial u}{R\partial\theta}+\frac{\partial v}{\partial x}+\frac{\partial w}{\partial x}\frac{\partial w}{R\partial\theta}\right)-B_{66}\left(\frac{2\partial^2 w}{R\partial\theta\partial x}-\frac{2\partial v}{R\partial x}\right)\right)=I_0\frac{\partial^2 u}{\partial t^2}, \tag{36}$$

$$\delta v: \frac{\partial}{R\partial\theta}\left(A_{12}\left(\frac{\partial u}{\partial x}+\frac{1}{2}\left(\frac{\partial w}{\partial x}\right)^2\right)+A_{22}\left(\frac{\partial v}{R\partial\theta}+\frac{w}{R}+\frac{1}{2}\left(\frac{\partial w}{R\partial\theta}\right)^2\right)-B_{12}\left(\frac{\partial^2 w}{\partial x^2}\right)-B_{22}\left(\frac{\partial^2 w}{R^2\partial\theta^2}-\frac{\partial v}{R^2\partial\theta}\right)\right)$$
$$+\frac{\partial}{\partial x}\left(A_{66}\left(\frac{\partial u}{R\partial\theta}+\frac{\partial v}{\partial x}+\frac{\partial w}{\partial x}\frac{\partial w}{R\partial\theta}\right)-B_{66}\left(\frac{2\partial^2 w}{R\partial\theta\partial x}-\frac{2\partial v}{R\partial x}\right)\right)$$
$$+\frac{\partial}{R^2\partial\theta}\left(B_{12}\left(\frac{\partial u}{\partial x}+\frac{1}{2}\left(\frac{\partial w}{\partial x}\right)^2\right)+B_{22}\left(\frac{\partial v}{R\partial\theta}+\frac{w}{R}+\frac{1}{2}\left(\frac{\partial w}{R\partial\theta}\right)^2\right)-D_{12}\left(\frac{\partial^2 w}{\partial x^2}\right)-D_{22}\left(\frac{\partial^2 w}{R^2\partial\theta^2}-\frac{\partial v}{R^2\partial\theta}\right)\right)$$
$$+\frac{\partial}{R\partial x}\left(B_{66}\left(\frac{\partial u}{R\partial\theta}+\frac{\partial v}{\partial x}+\frac{\partial w}{\partial x}\frac{\partial w}{R\partial\theta}\right)-D_{66}\left(\frac{2\partial^2 w}{R\partial\theta\partial x}-\frac{2\partial v}{R\partial x}\right)\right)=I_0\frac{\partial^2 v}{\partial t^2}, \tag{37}$$

$$\delta w: \frac{\partial^2}{\partial x^2}\left(\left(B_{11}\left(\frac{\partial u}{\partial x}+\frac{1}{2}\left(\frac{\partial w}{\partial x}\right)^2\right)+B_{12}\left(\frac{\partial v}{R\partial\theta}+\frac{w}{R}+\frac{1}{2}\left(\frac{\partial w}{R\partial\theta}\right)^2\right)-D_{11}\left(\frac{\partial^2 w}{\partial x^2}\right)-D_{12}\left(\frac{\partial^2 w}{R^2\partial\theta^2}-\frac{\partial v}{R^2\partial\theta}\right)\right)\right)$$
$$+\frac{\partial^2}{R^2\partial\theta^2}\left(B_{12}\left(\frac{\partial u}{\partial x}+\frac{1}{2}\left(\frac{\partial w}{\partial x}\right)^2\right)+B_{22}\left(\frac{\partial v}{R\partial\theta}+\frac{w}{R}+\frac{1}{2}\left(\frac{\partial w}{R\partial\theta}\right)^2\right)-D_{12}\left(\frac{\partial^2 w}{\partial x^2}\right)-D_{22}\left(\frac{\partial^2 w}{R^2\partial\theta^2}-\frac{\partial v}{R^2\partial\theta}\right)\right)$$
$$+\frac{2\partial^2}{R\partial x\partial\theta}\left(B_{66}\left(\frac{\partial u}{R\partial\theta}+\frac{\partial v}{\partial x}+\frac{\partial w}{\partial x}\frac{\partial w}{R\partial\theta}\right)-D_{66}\left(\frac{2\partial^2 w}{R\partial\theta\partial x}-\frac{2\partial v}{R\partial x}\right)\right)$$
$$-\frac{1}{R}\left(A_{12}\left(\frac{\partial u}{\partial x}+\frac{1}{2}\left(\frac{\partial w}{\partial x}\right)^2\right)+A_{22}\left(\frac{\partial v}{R\partial\theta}+\frac{w}{R}+\frac{1}{2}\left(\frac{\partial w}{R\partial\theta}\right)^2\right)-B_{12}\left(\frac{\partial^2 w}{\partial x^2}\right)-B_{22}\left(\frac{\partial^2 w}{R^2\partial\theta^2}-\frac{\partial v}{R^2\partial\theta}\right)\right)$$
$$+\left[-\rho_f h_f\left(\frac{\partial^2 w}{\partial t^2}+2v_x\frac{\partial^2 w}{\partial x\partial t}+v_x^2\frac{\partial^2 w}{\partial x^2}\right)+\frac{h_f}{R^2}\frac{\partial}{\partial\theta}\left(\mu\left(\frac{\partial^2 w}{\partial\theta\partial t}+v_x\frac{\partial^2 w}{\partial\theta\partial x}\right)\right)-\frac{2h_f}{R}\left(\mu\left(\frac{\partial w}{\partial t}+v_x\frac{\partial w}{\partial x}\right)\right)\right.$$
$$\left.+h_f\frac{\partial}{\partial x}\left(\mu\left(\frac{\partial^2 w}{\partial x\partial t}+v_x\frac{\partial^2 w}{\partial x^2}\right)\right)\right]-K_w w+K_{g\xi}\left(\cos^2\theta\frac{\partial^2 w}{\partial x^2}+2\cos\theta\sin\theta\frac{\partial^2 w}{R\partial x\partial\theta}+\sin^2\theta\frac{\partial^2 w}{R^2\partial\theta^2}\right)$$
$$+K_{g\eta}\left(\sin^2\theta\frac{\partial^2 w}{\partial x^2}-2\sin\theta\cos\theta\frac{\partial^2 w}{R\partial x\partial\theta}+\cos^2\theta\frac{\partial^2 w}{R^2\partial\theta^2}\right)=\rho h\frac{\partial^2 w}{\partial t^2}, \tag{38}$$

3. DQM

In this method, the differential equations are changed into a first order algebraic equation by employing appropriate weighting coefficients. Because weighting coefficients do not relate to any

special problem and only depend on the grid spacing. In other words, the partial derivatives of a function (say w here) are approximated with respect to specific variables (say x and θ), at a discontinuous point in a defined domain as a set of linear weighting coefficients and the amount represented by the function itself at that point and other points throughout the domain. The approximation of the n^{th} and m^{th} derivatives function with respect to x and y, respectively may be expressed in general form as (Shu and Du 1997)

$$\begin{aligned} f_x^{(n)}(x_i,\theta_i) &= \sum_{k=1}^{N_x} A^{(n)}{}_{ik} f(x_k,\theta_j), \\ f_\theta^{(m)}(x_i,\theta_i) &= \sum_{l=1}^{N_\theta} B^{(m)}{}_{jl} f(x_i,\theta_l), \\ f_{x\theta}^{(n+m)}(x_i,\theta_i) &= \sum_{k=1}^{N_x} \sum_{l=1}^{N_\theta} A^{(n)}{}_{ik} B^{(m)}{}_{jl} f(x_k,\theta_l), \end{aligned} \tag{39}$$

where N_x and N_θ, denotes the number of points in x and θ directions, $f(x,\theta)$ is the function and A_{ik}, B_{jl} are the weighting coefficients defined as

$$\begin{aligned} A^{(1)}{}_{ij} &= \frac{M(x_i)}{(x_i - x_j)M(x_j)}, \\ B^{(1)}{}_{ij} &= \frac{P(\theta_i)}{(\theta_i - \theta_j)M(\theta_j)}, \end{aligned} \tag{40}$$

where M and P are Lagrangian operators defined as

$$\begin{aligned} M(x_i) &= \prod_{j=1}^{N_x} (x_i - x_j), \quad i \neq j \\ P(\theta_i) &= \prod_{j=1}^{N_\theta} (\theta_i - \theta_j), \quad i \neq j. \end{aligned} \tag{41}$$

The weighting coefficients for the second, third and fourth derivatives are determined via matrix multiplication

$$\begin{aligned} A^{(2)}{}_{ij} &= \sum_{k=1}^{N_x} A^{(1)}{}_{ik} A^{(1)}{}_{kj}, \; A^{(3)}{}_{ij} = \sum_{k=1}^{N_x} A^{(2)}{}_{ik} A^{(1)}{}_{kj}, \; A^{(4)}{}_{ij} = \sum_{k=1}^{N_x} A^{(3)}{}_{ik} A^{(1)}{}_{kj}, \quad i,j = 1,2,...,N_x, \\ B^{(2)}{}_{ij} &= \sum_{k=1}^{N_\theta} B^{(1)}{}_{ik} B^{(1)}{}_{kj}, \; B^{(3)}{}_{ij} = \sum_{k=1}^{N_\theta} B^{(2)}{}_{ik} B^{(1)}{}_{kj}, \; B^{(4)}{}_{ij} = \sum_{k=1}^{N_\theta} B^{(3)}{}_{ik} B^{(1)}{}_{kj}, \quad i,j = 1,2,...,N_\theta. \end{aligned} \tag{42}$$

Using the following rule, the distribution of grid points in domain is calculated as

$$x_i = \frac{L_x}{2}[1-\cos(\frac{\pi i}{N_x})],$$
$$\theta_j = \frac{2\pi}{2}[1-\cos(\frac{\pi j}{N_\theta})], \tag{43}$$

The solution of the motion equations can be assumed as follows

$$u(x,\theta,t) = u_0(x,\theta)e^{\omega\tau}, \tag{44}$$

$$v(x,\theta,t) = v_0(x,\theta)e^{\omega\tau}, \tag{45}$$

$$w(x,\theta,t) = w_0(x,\theta)e^{\omega\tau}, \tag{46}$$

where $\omega = \lambda h\sqrt{\frac{\rho_f}{E}}$ and $\tau = \frac{t}{h}\sqrt{\frac{E}{\rho_f}}$ are the dimensionless natural frequency and dimensionless time. Substituting Eqs. (39) and (44)-(46) into the governing equations turns it into a set of algebraic equations expressed as

$$\begin{aligned}
&\delta u: A_{11}\left(\sum_{k=1}^{N_x} A^{(2)}{}_{ik}\,u(x_k,\theta_j)+\sum_{k=1}^{N_x} A^{(1)}{}_{ik}\,w(x_k,\theta_m)\sum_{k=1}^{N_x} A^{(2)}{}_{mk}\,w(x_k,\theta_j)\right)+\frac{A_{12}}{R^2}\left(R\sum_{k=1}^{N_x}\sum_{l=1}^{N_\theta} A^{(1)}{}_{ik}B^{(1)}{}_{jl}v(x_k,\theta_l)\right.\\
&+R\sum_{k=1}^{N_x} A^{(1)}{}_{ik}\,w(x_k,\theta_j)+\sum_{l=1}^{N_\theta} B^{(1)}{}_{il}\,w(x_l,\theta_m)\sum_{k=1}^{N_x}\sum_{l=1}^{N_\theta} A^{(1)}{}_{mk}B^{(1)}{}_{jl}w(x_k,\theta_l)\Big)-B_{11}\sum_{k=1}^{N_x} A^{(3)}{}_{ik}\,w(x_k,\theta_j)-\\
&\frac{B_{12}}{R^2}\sum_{k=1}^{N_x}\left(\sum_{l=1}^{N_\theta} A^{(1)}{}_{ik}B^{(2)}{}_{jl}\,w(x_k,\theta_l)-\sum_{l=1}^{N_\theta} B^{(2)}{}_{ik}\,v(x_k,\theta_j)\right)+\frac{A_{66}}{R^2}\left(\sum_{l=1}^{N_\theta} B^{(2)}{}_{il}u(x_l,\theta_j)\right.\\
&+R\sum_{k=1}^{N_x}\sum_{l=1}^{N_\theta} A^{(1)}{}_{ik}B^{(1)}{}_{jl}v(x_k,\theta_l)+\sum_{l=1}^{N_\theta} B^{(1)}{}_{il}\,w(x_l,\theta_m)\sum_{k=1}^{N_x}\sum_{l=1}^{N_\theta} A^{(1)}{}_{mk}B^{(1)}{}_{jl}w(x_k,\theta_l)\\
&\left.+\sum_{k=1}^{N_x} A^{(1)}{}_{ik}\,w(x_k,y_m)\sum_{l=1}^{N_\theta} B^{(2)}{}_{ml}w(x_l,\theta_j)\right)-\frac{2B_{66}}{R^2}\left(\sum_{k=1}^{N_x}\sum_{l=1}^{N_\theta} A^{(1)}{}_{ik}B^{(2)}{}_{jl}w(x_k,\theta_l)-\sum_{k=1}^{N_x}\sum_{l=1}^{N_\theta} A^{(1)}{}_{ik}B^{(1)}{}_{jl}v(x_k,\theta_l)\right)\\
&=\omega^2\left(\rho h u(x_i,\theta_j)\right),
\end{aligned} \tag{47}$$

$$\delta v: \frac{A_{12}}{R}\left(\sum_{k=1}^{N_x}\sum_{l=1}^{N_\theta} A^{(1)}{}_{ik}B^{(1)}{}_{jl}u(x_k,\theta_l)+\sum_{k=1}^{N_x}A^{(1)}{}_{ik}\,w(x_k,\theta_m)\sum_{k=1}^{N_x}\sum_{l=1}^{N_\theta}A^{(1)}{}_{mk}B^{(1)}{}_{jl}w(x_k,\theta_l)\right)+\frac{A_{22}}{R^3}\left(R\sum_{l=1}^{N_\theta}B^{(2)}{}_{il}v(x_l,\theta_j)\right.$$
$$\left.+R\sum_{l=1}^{N_\theta}B^{(1)}{}_{il}w(x_l,\theta_j)+\sum_{l=1}^{N_\theta}B^{(1)}{}_{il}\,w(x_l,\theta_m)\sum_{l=1}^{N_\theta}B^{(2)}{}_{ml}w(x_l,\theta_j)\right)-\frac{B_{22}}{R^3}\left(\sum_{l=1}^{N_\theta}B^{(3)}{}_{il}w(x_l,\theta_j)+\sum_{l=1}^{N_\theta}B^{(2)}{}_{il}v(x_l,\theta_j)\right)-$$
$$\frac{B_{12}}{R}\sum_{k=1}^{N_x}\sum_{l=1}^{N_\theta}A^{(2)}{}_{ik}B^{(1)}{}_{jl}\,w(x_k,\theta_l)+\frac{A_{66}}{R}\left(R\sum_{k=1}^{N_x}A^{(2)}{}_{ik}v(x_k,\theta_j)+\sum_{k=1}^{N_x}\sum_{l=1}^{N_\theta}A^{(1)}{}_{ik}B^{(1)}{}_{jl}u(x_k,\theta_l)\right.$$
$$\left.+\sum_{l=1}^{N_\theta}B^{(1)}{}_{il}\,w(x_l,\theta_m)\sum_{k=1}^{N_x}A^{(2)}{}_{mk}\,w(x_k,\theta_j)+\sum_{k=1}^{N_x}A^{(1)}{}_{ik}\,w(x_k,\theta_m)\sum_{k=1}^{N_x}\sum_{l=1}^{N_\theta}A^{(1)}{}_{mk}B^{(1)}{}_{jl}w(x_k,\theta_l)\right)$$
$$-\frac{2B_{66}}{R}\left(\sum_{k=1}^{N_x}A^{(2)}{}_{ik}\,v(x_l,\theta_j)+\sum_{k=1}^{N_x}\sum_{l=1}^{N_\theta}A^{(2)}{}_{ik}B^{(1)}{}_{jl}\,w(x_k,\theta_l)\right)$$
$$+\frac{B_{12}}{R^2}\left(\sum_{k=1}^{N_x}\sum_{l=1}^{N_\theta}A^{(1)}{}_{ik}B^{(1)}{}_{jl}u(x_k,\theta_l)+\sum_{k=1}^{N_x}A^{(1)}{}_{ik}\,w(x_k,\theta_m)\sum_{k=1}^{N_x}\sum_{l=1}^{N_\theta}A^{(1)}{}_{mk}B^{(1)}{}_{jl}w(x_k,\theta_l)\right)+\frac{B_{22}}{R^3}\left(R\sum_{l=1}^{N_\theta}B^{(2)}{}_{il}v(x_l,\theta_j)\right.$$
$$\left.+R\sum_{l=1}^{N_\theta}B^{(1)}{}_{il}w(x_l,\theta_j)+\sum_{l=1}^{N_\theta}B^{(1)}{}_{il}\,w(x_l,\theta_m)\sum_{l=1}^{N_\theta}B^{(2)}{}_{ml}w(x_l,\theta_j)\right)-\frac{D_{22}}{R^4}\left(\sum_{l=1}^{N_\theta}B^{(3)}{}_{il}w(x_l,\theta_j)+\sum_{l=1}^{N_\theta}B^{(2)}{}_{il}v(x_l,\theta_j)\right)-$$
$$\frac{D_{12}}{R^2}\sum_{k=1}^{N_x}\sum_{l=1}^{N_\theta}A^{(2)}{}_{ik}B^{(1)}{}_{jl}\,w(x_k,\theta_l)+\frac{B_{66}}{R^2}\left(R\sum_{k=1}^{N_x}A^{(2)}{}_{ik}v(x_k,\theta_j)+\sum_{k=1}^{N_x}\sum_{l=1}^{N_\theta}A^{(1)}{}_{ik}B^{(1)}{}_{jl}u(x_k,\theta_l)\right.$$
$$\left.+\sum_{l=1}^{N_\theta}B^{(1)}{}_{il}\,w(x_l,\theta_m)\sum_{k=1}^{N_x}A^{(2)}{}_{mk}\,w(x_k,\theta_j)+\sum_{k=1}^{N_x}A^{(1)}{}_{ik}\,w(x_k,\theta_m)\sum_{k=1}^{N_x}\sum_{l=1}^{N_\theta}A^{(1)}{}_{mk}B^{(1)}{}_{jl}w(x_k,\theta_l)\right)$$
$$-\frac{2D_{66}}{R^2}\left(\sum_{k=1}^{N_x}A^{(2)}{}_{ik}\,v(x_l,\theta_j)+\sum_{k=1}^{N_x}\sum_{l=1}^{N_\theta}A^{(2)}{}_{ik}B^{(1)}{}_{jl}\,w(x_k,\theta_l)\right)=\omega^2\left(\rho h v(x_i,\theta_j)\right), \tag{48}$$

$$\delta w: B_{11}\left(\sum_{k=1}^{N_x} A^{(3)}{}_{ik}\, u(x_k,\theta_j)+\sum_{k=1}^{N_x} A^{(1)}{}_{ik}\, w(x_k,\theta_m)\sum_{k=1}^{N_x} A^{(3)}{}_{mk}\, w(x_k,\theta_j)+\sum_{k=1}^{N_x} A^{(2)}{}_{ik}\, w(x_k,\theta_m)\sum_{k=1}^{N_x} A^{(2)}{}_{mk}\, w(x_k,\theta_j)\right)$$
$$+\frac{B_{12}}{R^2}\left(R\sum_{k=1}^{N_x}\sum_{l=1}^{N_\theta} A^{(2)}{}_{ik}B^{(1)}{}_{jl}\, v(x_k,\theta_l)+R\sum_{k=1}^{N_x} A^{(2)}{}_{ik}\, w(x_k,\theta_j)+\sum_{l=1}^{N_\theta} B^{(1)}{}_{il}\, w(x_l,\theta_m)\sum_{k=1}^{N_x}\sum_{l=1}^{N_\theta} A^{(2)}{}_{mk}B^{(1)}{}_{jl}\, w(x_k,\theta_l)\right.$$
$$\left.\sum_{k=1}^{N_x}\sum_{l=1}^{N_\theta} A^{(1)}{}_{ik}B^{(1)}{}_{jl}\, w(x_k,\theta_l)\sum_{k=1}^{N_x}\sum_{l=1}^{N_\theta} A^{(1)}{}_{mk}B^{(1)}{}_{jl}\, w(x_k,\theta_l)\right)-D_{11}\sum_{k=1}^{N_x} A^{(4)}{}_{ik}\, w(x_k,\theta_j)$$
$$-\frac{D_{12}}{R^2}\left(\sum_{k=1}^{N_x}\sum_{l=1}^{N_\theta} A^{(2)}{}_{ik}B^{(2)}{}_{jl}\, w(x_k,\theta_l)-\sum_{k=1}^{N_x}\sum_{l=1}^{N_\theta} A^{(2)}{}_{ik}B^{(1)}{}_{jl}\, v(x_k,\theta_l)\right)$$
$$+\frac{B_{12}}{R^2}\left(\sum_{k=1}^{N_x}\sum_{l=1}^{N_\theta} A^{(1)}{}_{ik}B^{(2)}{}_{jl}\, u(x_k,\theta_l)+\sum_{k=1}^{N_x} A^{(1)}{}_{ik}\, w(x_k,\theta_m)\sum_{k=1}^{N_x}\sum_{l=1}^{N_\theta} A^{(1)}{}_{mk}B^{(2)}{}_{jl}\, w(x_k,\theta_l)\right.$$
$$\left.+\sum_{k=1}^{N_x}\sum_{l=1}^{N_\theta} A^{(1)}{}_{ik}B^{(1)}{}_{ml}\, w(x_k,\theta_l)\sum_{k=1}^{N_x}\sum_{l=1}^{N_\theta} A^{(1)}{}_{mik}B^{(1)}{}_{jl}\, w(x_k,\theta_l)\right\}$$
$$+\frac{B_{22}}{R^4}\left(R\sum_{k=1}^{N_\theta} B^{(3)}{}_{ik}\, v(x_k,\theta_j)+R\sum_{k=1}^{N_\theta} B^{(2)}{}_{ik}\, w(x_k,\theta_j)+\sum_{l=1}^{N_\theta} B^{(3)}{}_{il}\, w(x_l,\theta_j)\sum_{l=1}^{N_\theta} B^{(2)}{}_{il}\, w(x_l,\theta_m)\sum_{l=1}^{N_\theta} B^{(2)}{}_{ml}\, w(x_l,\theta_j)\right)$$
$$-\frac{D_{12}}{R^2}\sum_{k=1}^{N_x}\sum_{l=1}^{N_\theta} A^{(2)}{}_{ik}B^{(2)}{}_{jl}\, w(x_k,\theta_l)-\frac{D_{22}}{R^4}\left(\sum_{k=1}^{N_\theta} B^{(4)}{}_{ik}\, w(x_k,\theta_j)-\sum_{k=1}^{N_\theta} B^{(3)}{}_{ik}\, v(x_k,\theta_j)\right)$$
$$+\frac{2B_{66}}{R^2}\left(\sum_{k=1}^{N_x}\sum_{l=1}^{N_\theta} A^{(1)}{}_{ik}B^{(2)}{}_{jl}\, u(x_k,\theta_l)+R\sum_{k=1}^{N_x}\sum_{l=1}^{N_\theta} A^{(2)}{}_{ik}B^{(1)}{}_{jl}\, v(x_k,\theta_l)+\sum_{k=1}^{N_x}\sum_{l=1}^{N_\theta} A^{(2)}{}_{ik}B^{(1)}{}_{ml}\, w(x_k,\theta_l)\sum_{l=1}^{N_\theta} B^{(1)}{}_{ml}\, w(x_l,\theta_j)\right.$$
$$+\sum_{k=1}^{N_x} A^{(2)}{}_{ik}\, w(x_k,\theta_m)\sum_{l=1}^{N_\theta} B^{(2)}{}_{ml}\, w(x_l,\theta_j)+\sum_{k=1}^{N_x}\sum_{l=1}^{N_\theta} A^{(1)}{}_{ik}B^{(1)}{}_{ml}\, w(x_k,\theta_l)\sum_{k=1}^{N_x}\sum_{l=1}^{N_\theta} A^{(1)}{}_{mk}B^{(1)}{}_{ml}\, w(x_k,\theta_l)$$
$$\left.+\sum_{k=1}^{N_x}\sum_{l=1}^{N_\theta} A^{(1)}{}_{ik}B^{(2)}{}_{ml}\, w(x_k,\theta_l)\sum_{l=1}^{N_x} A^{(1)}{}_{ml}\, w(x_l,\theta_j)\right)-\frac{D_{66}}{R^2}\left(\sum_{k=1}^{N_x}\sum_{l=1}^{N_\theta} A^{(2)}{}_{ik}B^{(2)}{}_{jl}\, w(x_k,\theta_l)-\sum_{k=1}^{N_x}\sum_{l=1}^{N_\theta} A^{(2)}{}_{ik}B^{(1)}{}_{jl}\, v(x_k,\theta_l)\right)$$
$$-\frac{A_{12}}{R}\left(\sum_{k=1}^{N_x} A^{(1)}{}_{ik}\, u(x_k,\theta_j)+0.5\sum_{k=1}^{N_x} A^{(1)}{}_{ik}\, w(x_k,\theta_m)\sum_{k=1}^{N_x} A^{(1)}{}_{ml}\, w(x_l,\theta_j)\right)-\frac{A_{22}}{R^3}\left(R\sum_{l=1}^{N_\theta} B^{(1)}{}_{il}\, w(x_l,\theta_j)+Rw(x_i,\theta_j)+\right.$$
$$\left.0.5\sum_{k=1}^{N_\theta} B^{(1)}{}_{ik}\, w(x_k,\theta_j)\sum_{k=1}^{N_\theta} B^{(1)}{}_{ik}\, w(x_k,\theta_j)\right)-\frac{B_{12}}{R}\left(\sum_{k=1}^{N_x} A^{(1)}{}_{ik}\psi_x(x_k,\theta_j)\right)-\frac{B_{22}}{R^2}\left(\sum_{k=1}^{N_\theta} B^{(1)}{}_{ij}\psi_\theta(x_j,\theta_j)\right)$$
$$+\frac{4E_{12}}{3h^2}\left(\sum_{k=1}^{N_x} A^{(1)}{}_{ik}\psi_x(x_k,\theta_j)+\sum_{k=1}^{N_x} A^{(2)}{}_{ik}\, w(x_k,\theta_j)\right)+\frac{4E_{22}}{3h^2R^2}\left(R\sum_{k=1}^{N_\theta} B^{(1)}{}_{ij}\psi_\theta(x_j,\theta_j)+\sum_{k=1}^{N_\theta} B^{(2)}{}_{ij}\, w(x_j,\theta_j)\right)$$
$$-\frac{2h_f}{R}\left(\mu\left(\dot{w}(x_i,\theta_j)+v_x\sum_{k=1}^{N_x} A^{(1)}{}_{ik}\, w(x_k,y_j)\right)\right)-\rho_f h_f\left(\ddot{w}(x_i,\theta_j)+2v_x\sum_{k=1}^{N_x} A^{(1)}{}_{ik}\,\dot{w}(x_k,\theta_j)+v_x^2\sum_{k=1}^{N_x} A^{(2)}{}_{ik}\, w(x_k,\theta_j)\right)$$
$$+\frac{h_f}{R^2}\left(\mu\left(\sum_{l=1}^{N_\theta} B^{(2)}{}_{il}\dot{w}(x_l,\theta_j)+v_x\sum_{k=1}^{N_x}\sum_{l=1}^{N_\theta} A^{(1)}{}_{ik}B^{(2)}{}_{jl}u(x_k,\theta_l)\right)\right)+h_f\left(\mu\left(\sum_{k=1}^{N_x} A^{(2)}{}_{ik}\,\dot{w}(x_k,y_j)+v_x\sum_{k=1}^{N_x} A^{(3)}{}_{ik}\, w(x_k,y_j)\right)\right)$$
$$-K_W w(x_i,\theta_j)+K_{g\xi}\left(\cos^2\theta\sum_{k=1}^{N_x} A^{(2)}{}_{ik}\, w(x_k,y_j)+\frac{2\cos\theta\sin\theta}{R}\sum_{k=1}^{N_x}\sum_{l=1}^{N_\theta} A^{(1)}{}_{ik}B^{(1)}{}_{jl}u(x_k,\theta_l)+\frac{\sin^2\theta}{R^2}\sum_{l=1}^{N_\theta} B^{(2)}{}_{il}\, w(x_l,\theta_j)\right)$$
$$+K_{g\eta}\left(\sin^2\theta\sum_{k=1}^{N_x} A^{(2)}{}_{ik}\, w(x_k,y_j)-\frac{2\sin\theta\cos\theta}{R}\sum_{k=1}^{N_x}\sum_{l=1}^{N_\theta} A^{(1)}{}_{ik}B^{(1)}{}_{jl}u(x_k,\theta_l)+\frac{\cos^2\theta}{R^2}\sum_{l=1}^{N_\theta} B^{(2)}{}_{il}\, w(x_l,\theta_j)\right)=\omega^2\left(\rho h w(x_i,\theta_j)\right), \tag{49}$$

Finally, the governing equations (i.e., Eqs. (47)- (49)) in matrix form can be expressed as

$$\left[[K_L]+[K_{NL}]+[M]\omega^2\right][d]=[0], \tag{50}$$

where $[d]=[u\ v\ w]^T$; $[K_L]$ and $[K_{NL}]$ are respectively, linear and nonlinear stiffness matrixes; and $[M]$ is the mass matrix.

However, using eigenvalue problem, the frequencies obtained from the solution of Eq. (50) are complex due to the damping existed in the presence of the viscous fluid flow. Hence, the results are containing two real and imaginary parts. The real part is corresponding to the system damping, and the imaginary part representing the system natural frequencies.

4. Numerical results and discussion

In this section, the effects of different parameters such as volume percent of CNTs, distribution type of CNTs, elastic medium and geometrical parameters of shell are shown on the frequency and critical fluid velocity of structure. For this purpose, a poly ethylene (PE) pipe with Yong modulus of $E=125\,GPa$, poison's ratio of $\upsilon=0.3$ and density of $\rho=1.45\,Kg/m^3$ is considered. In addition, the material properties of CNTs are chosen from Zhang *et al*. (2014b). The pipe is considered with three kinds of boundary conditions: simply supported at both ends (SS) or clamped (CC), and one end simply supported and another clamped (SC).

Figs. 2 and 3 show the effect of volume percent of CNTs on the dimensionless natural frequency ($\mathrm{Im}(\Omega=\omega R\sqrt{\rho/E})$) and damping ($\mathrm{Re}(\Omega)$) of pipe versus dimensionless flow velocity ($V=\sqrt{\rho_f/C_{11}}\,v_x$), respectively. As can be seen, $\mathrm{Im}(\Omega)$ decreases with increasing V, while the $\mathrm{Re}(\Omega)$ remains zero. These imply that the system is stable. When the natural frequency becomes zero, critical velocity is reached, which the system loses its stability due to the divergence via a pitchfork bifurcation. Hence, the eigen-frequencies have the positive real parts, which the system becomes unstable. In this state, both real and imaginary parts of frequency become zero at the same point. Therefore, with increasing flow velocity, system stability decreases and became susceptible to buckling. It can be observed that, the $\mathrm{Im}(\Omega)$ of system increases with increasing volume percent of CNTs due to increase in the stability of structure.

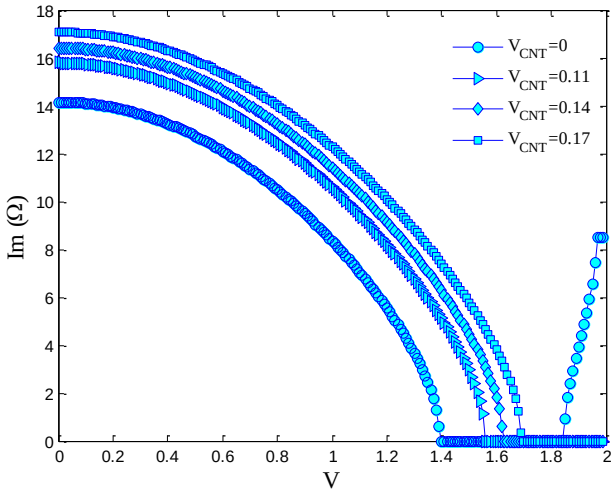

Fig. 2 Effects of CNT volume percent on the dimension frequency ($\mathrm{Im}(\omega)$) versus dimension flow velocity

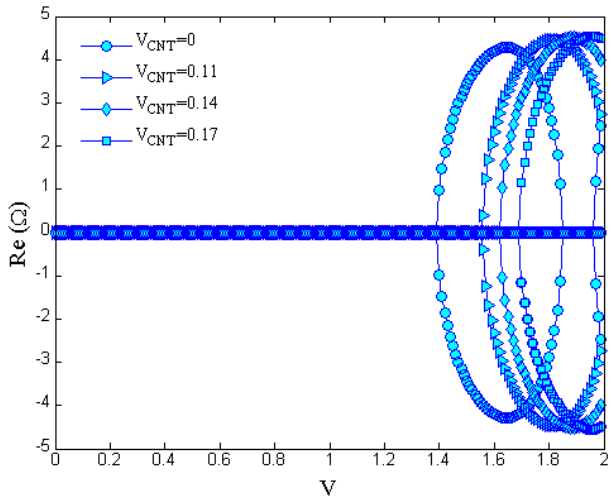

Fig. 3 Effects of CNT volume percent on the dimension frequency ($\mathrm{Re}(\omega)$) versus dimension flow velocity

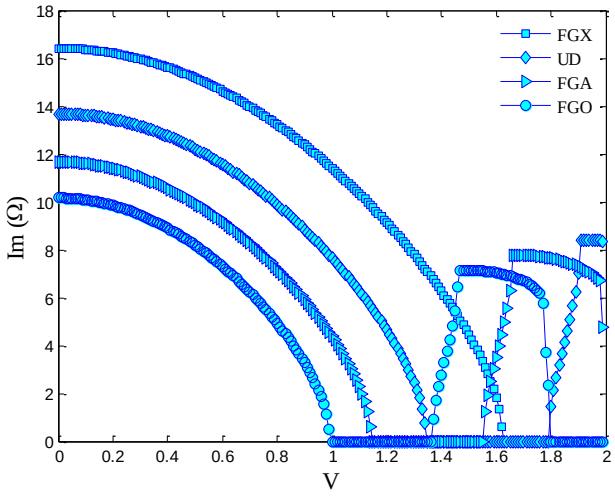

Fig. 4 Effects of CNT distribution type on the dimension frequency ($\mathrm{Im}(\omega)$) versus dimension flow velocity

Depicted in Figs. 4 and 5 is the non-dimensional frequency and damping for the UD and three types of FG CNTRC cylindrical shell versus dimensionless flow velocity. It should be noted that the mass fraction (w_{CNT}) of the UD and FG distribution of CNTs in polymer are considered equal for the purpose of comparisons. As can be seen, the frequency and critical fluid velocity of FGA-

and FGO- CNTRC cylindrical shell are smaller than those of UD-CNTRC cylindrical shell while the FGX- CNTRC cylindrical shell has higher frequency and critical fluid velocity with respect to three other cases. It is due to the fact that the stiffness of CNTRC cylindrical shell changes with the form of CNT distribution in matrix. However, it can be concluded that CNT distribution close to top and bottom are more efficient than those distributed nearby the mid-plane for increasing the stiffness of plates.

The dimensionless natural frequency and damping of the system are demonstrated in Figs. 6 and 7 for different elastic mediums. In this figure, four cases are considered as follows:

Case 1: $K_W = 0\ N/m^3, K_{g\xi} = 0\ N/m, K_{g\eta} = 0\ N/m$ → indicating without elastic medium.

Case 2: $K_W = 41.4\ N/m^3, K_{g\xi} = 0\ N/m, K_{g\eta} = 0\ N/m$ → indicating Winkler medium.

Case 3: $K_W = 41.4\ N/m^3, K_{g\xi} = 4.14\ N/m, K_{g\eta} = 4.14\ N/m$ →indicating Pasternak medium.

Case 4: $K_W = 41.4\ N/m^3, K_{g\xi} = 41.4\ N/m, K_{g\eta} = 4.14\ N/m, \theta = 45^0$ →indicating orthotropic Pasternak medium.

As can be seen, considering elastic medium increases natural frequency and critical fluid velocity of the system. It is due to the fact that considering elastic medium leads to stiffer structure. Furthermore, the effect of the Pasternak-type is higher than the Winkler-type on the natural frequency and critical fluid velocity of the pipe. It is perhaps due to the fact that the Winkler-type is capable to describe just normal load of the elastic medium while the Pasternak-type describes both transverse shear and normal loads of the elastic medium.

The effect of the different boundary conditions on the dimensionless natural frequency and damping of the pipe is depicted in Figs. 8 and 9. As can be seen, the natural frequency and critical fluid velocity of the pipe are maximum and minimum for CC and SS boundary conditions, respectively. It is because that considering CC boundary condition leads harder structure.

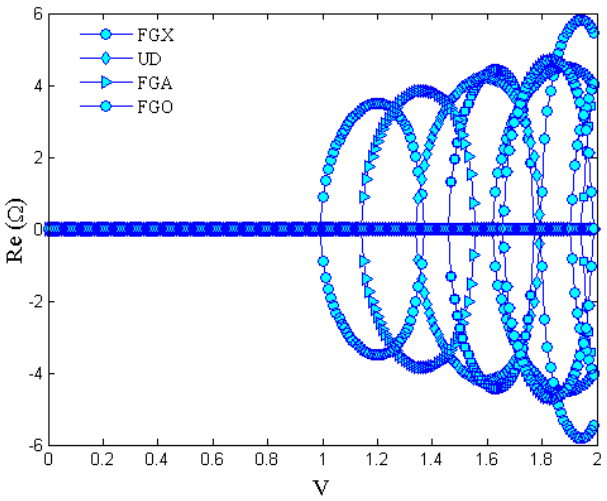

Fig. 5 Effects of CNT distribution type on the dimension frequency ($\mathrm{Re}(\omega)$) versus dimension flow velocity

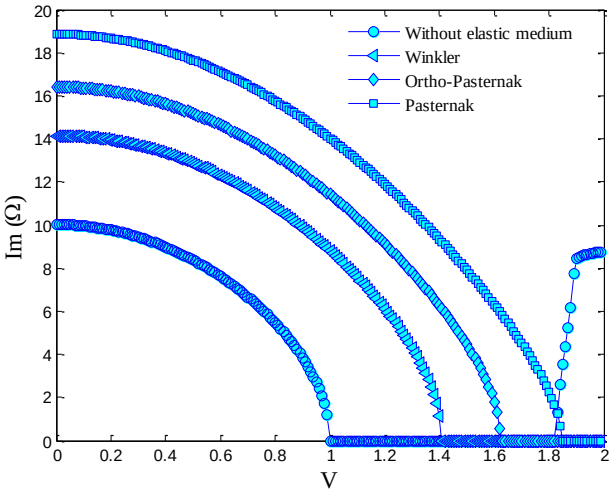

Fig. 6 Effects of elastic medium on the dimension frequency ($\mathrm{Im}(\omega)$) versus dimension flow velocity

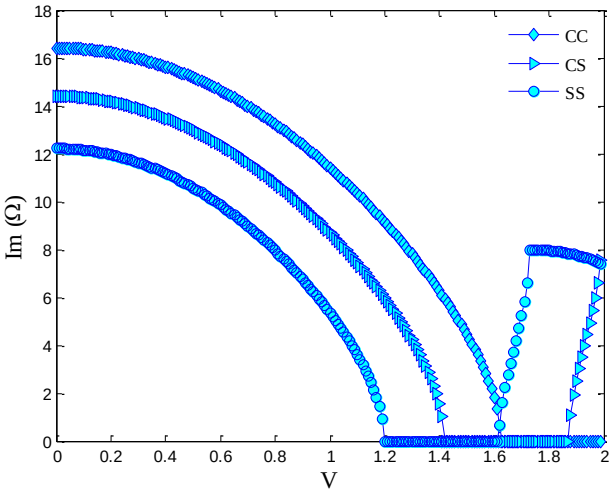

Fig. 7 Effects of boundary conditions on the dimension frequency ($\mathrm{Im}(\omega)$) versus dimension flow velocity

5. Conclusions

Internal fluid induced nonlinear vibration and instability of FG-CNT-reinforced pipe were presented in this study based on Flugge shell theory. CNT distributions in polymer were considered as UD, FGA, FGX and FGO. The rule of mixture was used for obtaining the material

properties of FG-CNTRC cylindrical shell. The surrounding elastic medium was simulated by orthotropic Pasternak foundation. Based on energy method and Hamilton's principle, the motion equations were derived. DQM is applied for obtaining the frequency and critical fluid velocity of system so that the effects of the volume percent of CNTs, elastic medium, distribution types of CNTs and boundary conditions were considered. Results indicate that considering elastic medium decreases frequency and critical fluid velocity of the FG-CNTRC shell. It was also concluded that frequency and critical fluid velocity get larger as the CNT volume fraction increases. Furthermore, the highest and lowest frequency and critical fluid velocity were respectively obtained for FGX- and FGO-CNTRC cylindrical shell.

References

Alizade, A.A., Mirdamadi, H.R. and Pishevar, A. (2016), "Reliability analysis of pipe conveying fluid with stochastic structural and fluid parameters", *Eng. Struct.*, **122**, 24-32.

Amabili, M. (2008), "*Nonlinear Vibrations and Stability of Shells and Plates*", CAMBRIDGE UNIVERSITY PRESS.

Amabili, M., Karagiozis, K. and Paidoussis, M.P. (2009), "Effect of geometric imperfections on non-linear stability of circular cylindrical shells conveying fluid", *Int. J. Nonlinear. Mech*., **44**(3), 276- 289.

Amabili, M., Pellicano, F. and Paidoussis, M.P. (2002), "Non-linear dynamics and stability of circular cylindrical shells conveying flowing fluid", *Comput. Struct*., **80**(9-10), 899-906,.

Firouz-Abadi, R.D., Noorian, M.A. and Haddadpour, H. (2010), "A fluid–structure interaction model for stability analysis of shells conveying fluid", *J. Fluid. Struct.*, **26**(5), 747-763.

He, T. (2015), "Partitioned coupling strategies for fluid-structure interaction with large displacement: Explicit, implicit and semi-implicit schemes", *Wind Struct*., **20**(3), 423-448.

Hu, K., Wang, Y.K., Dai, H.L., Wang, L. and Qian, Q. (2016), "Nonlinear and chaotic vibrations of cantilevered micropipes conveying fluid based on modified couple stress theory", *Int. J. Eng. Sci.*, **105**, 93-107.

Jafari Mehrabadi, S. and Sobhani Aragh, B. (2014), "Stress analysis of functionally graded open cylindrical shell reinforced by agglomerated carbon nanotubes", *Thin. Wall. Struct.*, **80**, 130-141.

Khalili, S.M.R., Davar, A. and Malekzadeh Fard, K. (2012), "Free vibration analysis of homogeneous isotropic circular cylindrical shells based on a new three-dimensional refined higher-order theory", *Int. J. Mech. Sci*., **56**(1), 1-25.

Kolahchi, R., Rabani Bidgoli, M., Beygipoor, Gh. and Fakhar, M.H. (2015), "A nonlocal nonlinear analysis for buckling in embedded FG-SWCNT-reinforced microplates subjected to magnetic field", *Int. J. Mech. Sci*., **29**(9), 3669-3677.

Kolahchi, R., Safari, M. and Esmailpour, M. (2016), "Dynamic stability analysis of temperature-dependent functionally graded CNT-reinforced visco-plates resting on orthotropic elastomeric medium", *Compos. Struct*., **150**, 255-265.

Kutlu, A. and Omurtag, M.H. (2012), "Large deflection bending analysis of elliptic plates on orthotropic elastic foundation with mixed finite element method", *Int. J. Mech. Sci*., **65**(1), 64-74.

Lei, Z.X., Zhang, L.W., Liew, K.M. and Yu, J.L. (2014), "Dynamic stability analysis of carbonnanotube-reinforced functionally graded cylindrical panels using the element-free kp-Ritz method", *Compos. Struct.*, **113**, 328-338.

Liew, K.M., Lei, Z.X., Yu, J.L. and Zhang, L.W. (2014), "Postbuckling of carbon nanotube-reinforced functionally graded cylindrical panels under axial compression using a meshless approach", *Comput. Meth. Appl. Mech. Eng*., **268**, 1-17.

Morgenthal, G. and McRobie, A. (2002), "A comparative study of numerical methods for fluid structure interaction analysis in long-span bridge design", *Wind Struct*., **5**(2), 101-114.

Nascimbene, R. (2013), "Analysis and optimal design of fiber-reinforced composite structures: sail against the wind", *Wind Struct.*, **16**(6), 541-560.
Park, K.J. and Kim, Y.W. (2016), "Vibration characteristics of fluid-conveying FGM cylindrical shells resting on Pasternak elastic foundation with an oblique edge", *Thin. Wall. Struct.*, **106**, 407-419.
Senthil Kumar, D. and Ganesan, N. (2008), "Dynamic analysis of conical shells conveying fluid", *J. Sound Vib.*, **310**(1-2), 38-57.
Shu, C. and Du, H. (1997), "Free vibration analysis of laminated composite cylindrical shells by DQM", *Compos. Part B: Eng.*, **28**(3), 267-274.
Thomas, B. and Roy, T. (2016), "Vibration analysis of functionally graded carbon nanotube-reinforced composite shell structures", *Acta Mech.*, **227**(2), 581-599.
Wang, L. and Ni, Q. (2009), "A reappraisal of the computational modelling of carbon nanotubes conveying viscous fluid", *Mech. Res. Commun.*, **36**(7), 833-837.
Zhang, L.W., Lei, Z.X., Liew, K.M. and Yu, J.L. (2014a), "Large deflection geometrically nonlinear analysis of carbon nanotube-reinforced functionally graded cylindrical panels", *Comput. Method. Appl. M.*, **273**, 1-18,.
Zhang, L.W., Lei, Z.X., Liew, K.M. and Yu, J.L. (2014b), "Static and dynamic of carbon nanotube reinforced functionally graded cylindrical panels", *Compos. Struct.*, **111**, 205-212.

CC